Investigating the hydromechanical behaviour of bentonite pellets by swelling pressure tests and discrete element modelling

Benjamin Darde, Jean-Noël Roux, Jean-Michel Pereira, Patrick Dangla, Jean Talandier, Minh Ngoc Vu, Anh Minh A.M. Tang

TITLE:

Investigating the hydromechanical behaviour of bentonite pellets by swelling pressure tests and discrete element modelling.

AUTHORS:

1) DARDE Benjamin
Affiliation : (1) Navier, Ecole des Ponts, Univ Gustave Eiffel, CNRS, Marne-la-Vallée, France; and (2) French National Radioactive Waste Management Agency (Andra), Châtenay-Malabry, France
Address: Ecole des Ponts ParisTech, Laboratoire Navier, 6-8 avenue Blaise Pascal, 77455 Marne-la-Vallée, France
Email: benjamin.darde@enpc.fr

2) ROUX Jean-Noël
Affiliation: Navier, Ecole des Ponts, Univ Gustave Eiffel, CNRS, Marne-la-Vallée, France
Address: Ecole des Ponts ParisTech, Laboratoire Navier, 2 allée Kepler, 77420 Champs-sur-Marne, France
Email: jean-noel.roux@ifsttar.fr

3) PEREIRA Jean-Michel
Affiliation: Navier, Ecole des Ponts, Univ Gustave Eiffel, CNRS, Marne-la-Vallée, France
Address: Ecole des Ponts ParisTech, Laboratoire Navier, 6-8 avenue Blaise Pascal, 77455 Marne-la-Vallée, France
Email: jean-michel.pereira@enpc.fr

4) DANGLA Patrick
Affiliation: Navier, Ecole des Ponts, Univ Gustave Eiffel, CNRS, Marne-la-Vallée, France
Address: Ecole des Ponts ParisTech, Laboratoire Navier, 6-8 avenue Blaise Pascal, 77455 Marne-la-Vallée, France
Email: patrick.dangla @ifsttar.fr

5) TALANDIER Jean
Affiliation: French National Radioactive Waste Management Agency (Andra), Châtenay-Malabry, France
Address: Andra, DRD/MFS, 1-7 rue Jean Monnet, Parc de la croix blanche, 92298 Châtenay-Malabry, France
Email: jean.talandier@andra.fr

6) VU Minh Ngoc
Affiliation: French National Radioactive Waste Management Agency (Andra), Châtenay-Malabry, France
Address: Andra, DRD/MFS, 1-7 rue Jean Monnet, Parc de la croix blanche, 92298 Châtenay-Malabry, France
Email: minh-ngoc.vu@andra.fr

7) TANG Anh Minh*
Affiliation: Navier, Ecole des Ponts, Univ Gustave Eiffel, CNRS, Marne-la-Vallée, France
Address: Ecole des Ponts ParisTech, Laboratoire Navier, 6-8 avenue Blaise Pascal, 77455 Marne-la-Vallée, France
Email: anh-minh.tang@enpc.fr

*Corresponding author.

ACKNOWLEDGEMENTS

The present work is supported by the French National Radioactive Waste Management Agency (Andra), which is gratefully acknowledged.

ABSTRACT

Bentonite pellet mixtures are candidate material for the sealing of galleries in radioactive waste disposals. The hydromechanical behaviour of assemblies of bentonite pellets is investigated upon partial hydration through (*i*) suction-controlled swelling pressure tests in the laboratory and (*ii*) discrete element method (DEM) simulations. The combination of these experimental and numerical approaches highlights that, before the mixture homogenisation, the swelling pressure develops in two phases. The first phase is characterised by an increase of contact forces between pellets. The second phase is characterised by plasticity at contacts between pellets and is controlled by the progressive decrease of pellet strength and stiffness upon hydration. In addition, numerical results highlight that the swelling pressure measured in the laboratory can be influenced by the sample preparation, the cell size, and the diameter of the pressure sensor.

Keywords: Expansive soils; Pellets; Swelling pressure; DEM simulations

1. Introduction

Compacted bentonite-based materials are a candidate material for engineered barriers in radioactive waste disposal concepts due to their low permeability, good radionuclide retention capacity and ability to swell upon hydration, resulting in the filling of technological voids and a swelling pressure development on the tunnel walls. The development of a swelling pressure contributes to the decrease of hydraulic conductivity in the excavation induced damaged zone. In this respect, the hydromechanical behaviour of compacted bentonite materials has been widely studied over the last two decades [1-16].

The use of pellet-based bentonite materials has been considered an interesting solution for the installation of engineered barriers because of operational convenience [17-27]. Pellet materials are laid as a dry granular assembly in the galleries and subsequently undergo swelling upon hydration from the host rock pore water. Upon hydration, pellet materials are known to lose their initial granular structure and reach a homogeneous final state [18, 19, 27]. Like other bentonite materials, the final swelling pressure developed by pellet materials in constant volume conditions can be estimated from their initial dry density [28, 29].

Before homogenisation, the hydromechanical behaviour of pellet materials is still not perfectly understood. Upon pellet swelling, the swelling pressure is influenced by the granular nature of the material [28, 29]. Interactions at contacts between pellets and stiffness decrease of the pellets during hydration are thought to control the overall hydromechanical behaviour [31].

It is proposed in the present study to evaluate the influence of interactions at contacts on the macroscopic response of bentonite pellet assemblies upon hydration. The objective is to obtain an insight into the hydromechanical behaviour of pellet materials upon hydration, before reaching a homogeneous state. In this purpose, swelling pressure tests are performed in the laboratory on pellet materials. Discrete Element Method (DEM) is then used to model the swelling pressure tests.

In DEM simulations [32], each grain is modelled individually. DEM allows to study the influence of the behaviour of one pellet and interactions at contacts between pellets on the behaviour of the granular assembly. DEM has been successfully used in similar engineering problems involving irreversible changes in the volume of grains, such as the effect of particle thermal expansion in granular materials [33, 34]; or grain-scale modelling of the swelling behaviour of absorbent polymer particles upon hydration in hygienic products [35].

The ability of DEM to access grain-scale phenomena can provide valuable information about the behaviour of assemblies of pellets upon hydration-induced pellet swelling. These latter can be obtained neither through experimental tests, since only macroscopic phenomena are measurable most of the time, nor through finite element method (FEM) simulations, which require a homogeneous continuum. In the present study, DEM is an interesting tool to study the hydromechanical behaviour of pellet materials before homogenisation while providing a better understanding of the results of laboratory tests.

The present paper applies DEM to the simulation of the partial hydration of expansive clay pellet assemblies. In DEM, the behaviour of each pellet is based on the hydromechanical model for a single pellet proposed by Darde et al. (2018) [36]. Interactions between pellets are described by contact mechanics and characterised by the Hertz law and the Coulomb friction [37]. Some preliminary results obtained using this approach can be found in Darde et al. (2020) [38]. In the present work, more comprehensive description, analysis and discussion of the experimental study and numerical simulations are presented. The modelling approach is validated by simulating suction-controlled swelling pressure tests carried out at laboratory scale.

Materials and experimental methods regarding the swelling pressure tests are first described. The main features of the DEM simulations are presented in the second part. Both experimental and numerical results are then presented and discussed in the third and fourth parts, respectively. Important contributions and main perspectives arising from the present study then constitute the paper conclusion.

2. Material and Experimental methods

2.1. Bentonite pellets

The material studied in the framework of the present study is an assembly of MX80 bentonite granules or pellets. MX80 is a sodium (Na)-bentonite from Wyoming (USA). Its main properties are summarised in Table 1.

Pellets are obtained from MX80 bentonite powder by pressure casting (compaction in a mould). Granules are composed of a central cylinder with spherical caps at both ends. Their initial dry density, suction value and water content are 1.90 g/cm^3, 89 MPa and 0.122, respectively [36]. The main initial properties of the pellets are listed in Figure 1 and Table 2.

2.2. Constant-volume swelling pressure tests

2.2.1. Pellet assembly

In the French concept of radioactive waste disposal, a bentonite pellet and powder (crushed pellets) mixture is candidate material for the sealing plugs preventing fluid migrations. The dry density of the reference mixture and the dry mass proportion of pellets and powder are 1.50 g/cm^3 and 70/30, respectively. The mixture is laid in a dry state as a granular assembly. Interactions between high-density granules are thought to have an influence on the material mechanical behaviour at the beginning of hydration, especially at the structure scale if heterogeneity of powder content arises [22], as a consequence of either an imperfect laying or particle segregation.

In the present work, the influence of the granular structure of the material on the macroscopic response at the beginning of hydration is studied through constant-volume swelling pressure tests carried out on a pellet assembly without powder. The material dry density in the present study is thus 1.05 g/cm^3. The initial pellet volume fraction is 0.553.

2.2.2. Isochoric cell

The swelling pressure in the present study is defined as the pressure developed by the material against the upper wall of a cylindrical isochoric cell upon hydration. A pressure sensor (BER-A-5MP15S from Kyowa, capacity of 5 MPa) at the centre of the cell upper wall measures the swelling pressure as a function of elapsed time.

The cylinder dimensions are given in Table 3. A sketch of the cell is presented in Figure 2.

2.2.3. Sample preparation

Two samples are prepared (referred to as SP1 and SP2 in the following). In both cases, the target dry density (1.05 g/cm^3) is reached by introducing a mass of pellets of 99.9 g. This mass corresponds to 209 pellets. The 209 pellets are placed one by one in the cell in successive layers [22]. Cells are then closed by placing the upper wall so that the cell height is 30 mm. The closure step can induce a pressure increase if upper wall-pellet contacts are created. The preparation step of SP1 and SP2 resulted in an initial pressure of 10 kPa and 55 kPa after the cell closure, respectively.

2.2.4. Suction-controlled hydration at constant room temperature

Hydration is performed step by step through the vapour equilibrium technique as described in [2, 19, 39]. Suction is decreased from 89 MPa (initial state) to 4 MPa (SP1 test) and 9 MPa (SP2 test). Salt solutions used in the study are listed in Table 4 along with their corresponding suction values.

A peristaltic pump makes air circulate through the salt solution to impose a constant target relative humidity, then through the isochoric cell. Humid air is allowed to circulate directly from the bottom to the top of the cell through a side tube. Thus, no excessive air pressure is developed when using the peristaltic pump and humid air is considered to circulate freely inside the inter-pellet porosity (Figure 3). Room temperature is 20°C ± 1°C.

As humid air circulates in the isochoric cell, pellets are hydrated and swell. Pellet swelling in an isochoric cell results in the development of a swelling pressure which is measured by the pressure sensor at the centre of the top wall.

Equilibrium is considered to be reached when the pressure measured by the sensor remains constant for a minimum of 3 days. The final pressure value is used to draw the suction-swelling pressure relationship. The current salt solution is then replaced by the following one (Table 4) to impose the next relative humidity step.

3. Discrete Element Method simulations of the swelling pressure tests

3.1. Overview of the method

DEM simulations are carried out by using an in-house program [40]. In the DEM simulations carried out, each pellet is modelled as a sphere. A molecular dynamics scheme in the quasistatic limit is used [40]. The hydromechanical behaviour of each pellet upon hydration is described by the model proposed by [36] for a single pellet.

The sphere diameter a_{eq} is chosen such that its volume coincides with the pellet volume V:

(1)
$$a_{eq} = \left(\frac{6\,V}{\pi}\right)^{1/3}$$

The initial value of a_{eq} is obtained from initial values of mass and density: $a_{eq\,0}$ =7.53 mm.

In order to assess the ability of the model to reproduce the hydromechanical behaviour of the granular assembly, swelling pressure tests are simulated. In the simulations, the isochoric cell is modelled as a rigid cylinder (infinite Young's modulus), the height and diameter of which are the same as the cell used for the swelling pressure tests. 209 pellets are simulated in each simulations, corresponding to the number of granules in the swelling pressure tests performed in the laboratory, thus the same pellet volume fraction.

Simulations are carried out in two main steps:

- the preparation step, corresponding to the installation of model beads inside the cylinder and the cell closure;
- the hydration steps.

Three different types of simulations are carried out and referred to as DEM1; DEM2; DEM3. For each type, 100 calculations are performed to quantify the variability of the results. The difference between the simulations is the initial position of the beads following the sample preparation. This point is described in a dedicated section. DEM1 simulations aim at reproducing the swelling pressure tests with optimised preparation to avoid initial pressure (no friction during preparation). DEM2 simulations aim at assessing the influence of a less optimised initial state following the preparation step on the material behaviour upon hydration (friction during preparation). In both DEM1 and DEM2, contact friction is taken into account during hydration. In DEM3 simulations, no contact friction is taken into account during both preparation and hydration steps (Table 5).

The following parts provide details concerning the model for a pellet, contact laws, hydration and preparation steps.

3.2. Hydromechanical behaviour of a pellet

From grain-level experimental characterisation, Darde et al. (2018) [36] proposed a model describing the evolution of pellet stiffness, volumetric strain and strength upon suction decrease (Figures 4a and 4b). Pellets are characterised by their microstructure, assumed to be fully-saturated. The following notations are used for the model parameters:

- E_m is the pellet Young modulus;
- v is the pellet Poisson ratio, taken equal to 0.3;
- ε_{Vm} is the volumetric strain;
- s_0 is the initial pellet suction;
- R_A is the strength;
- α_m; β_m and C_A are model parameters, respectively taken equal to 0.024 MPa^{-1}; 0.016 MPa^{-1} and 0.12 N/MPa [36];
- p' is the effective mean stress. Since pellets are considered fully-saturated, p' is taken equal to the sum of the total mean stress p and the suction s. In the considered suction range, $s \gg p$ and it is assumed that $p' = s$.

Using these notations, the model equations describing the pellet behaviour are:

(2) $$E_m(p') = 3(1-2\nu)\frac{1}{\beta_m}\exp(\alpha_m p')$$

(3) $$\varepsilon_{Vm}(p') = \frac{\beta_m}{\alpha_m}[\exp(-\alpha_m s_0) - \exp(-\alpha_m p')]$$

(4) $$R_A(p') = C_A\, E_m(p')$$

(5) $$p' = p + s = s$$

The above equations are used in DEM to determine the mechanical properties of each particle at any value of suction.

3.3. Hydration modelling

Pellet hydration and subsequent swelling are simulated by a simultaneous increase of all the bead diameters. It is therefore assumed that all pellets get hydrated at the same rate. The diameter increase at each hydration step *i* varies from 0.1 % to 0.9 % from initial state (89 MPa of suction) to final state (9 MPa of suction). 60 diameter increments are imposed, for an overall diameter increase of ~15 %:

$$a_{eq\ \mathrm{i+1}} = \lambda_i\ a_{eq\ \mathrm{i}} \quad (6)$$

Where:

$$\lambda_i = \exp\left[\ln\left(\frac{\lambda_f}{\lambda_0}\right)\left(\frac{a_{eq\ i} - a_{eq\ 0}}{a_{eq\ f} - a_{eq\ 0}}\right) + \ln(\lambda_0)\right] \quad (7)$$

Where λ_i characterises the diameter increment; λ_f and λ_0 are parameters taken equal to 10^{-2} and 10^{-3}, respectively; $a_{eq\ i}$ and $a_{eq\ f}$ are the equivalent diameters at step *i* and at the final suction value, respectively.

From radius increments, the volume variation is obtained. The suction value corresponding to each hydration stage is obtained from equation (3). Stiffness and strength are obtained from equations (2) and (4), respectively.

Contact laws then allow the granular assembly evolution to be computed, taking into account the suction-dependency of the aforementioned material parameters.

3.4. Contact laws

In contacts between two granules of same radius and modulus, the Hertz law (Figure 5) relates the normal contact elastic force F_N to the normal elastic deflection at contact δ_N^e as:

$$F_N = \frac{1}{3}\frac{E_m}{1-\nu^2}\ a_{eq}{}^{1/2}\ \delta_N^{e\ \ 3/2} \quad (8)$$

Contacts between a granule and the infinitely stiff flat walls satisfy:

(9)
$$F_N = \frac{2^{3/2}}{3}\frac{E_m}{1-\nu^2}\ {a_{eq}}^{1/2}\ {\delta_N^e}^{\ 3/2}$$

Granule strength is taken into account by considering perfect plasticity at contacts. The elastic part is described by the Hertz law (equations (8) and (9)) and the elastic limit is given by equation (4). Thus,

(10)
$$F_N \leq R_A$$

and plastic deflection can arise for $F_N = R_A$ (Figure 6a).

Tangential elasticity at contacts is described by a simplified form of the Cattaneo-Mindlin-Deresiewicz laws [37], with due care for energetic consistency and objectivity, as proposed by Agnolin and Roux (2007) [40]. $\dot{\boldsymbol{F}}_{\boldsymbol{T}}$, the increment of tangential reaction vector $\boldsymbol{F_T}$, is related to $\dot{\boldsymbol{\delta}}_{\boldsymbol{T}}$, the increment of relative tangential displacement vector $\boldsymbol{\delta_T}$, using the following equation:

(11)
$$\dot{\boldsymbol{F}}_{\boldsymbol{T}} = \frac{2-2\nu}{2-\nu}\frac{\mathrm{d}F_N}{\mathrm{d}\delta_N}\ \ \dot{\boldsymbol{\delta}}_{\boldsymbol{T}}$$

The Coulomb condition is checked so that

(12)
$$F_T \leq \mu\ F_N$$

where F_T is the norm of the $\boldsymbol{F_T}$ vector and μ is a friction coefficient.
Sliding can arise for $F_T = \mu\ F_N$ (Figure 6b). The same value of μ is taken for both pellet-pellet and pellet-wall contacts.

Damping is taken into account by adding a viscous component to the hertzian elastic force. The viscous force, N^v, in a contact between two pellets is written as:

(13)
$$N^v = \alpha_v \left(2\, m_p \frac{\mathrm{d}F_N}{\mathrm{d}\delta_N}\right)^{1/2} \frac{\mathrm{d}\delta_N}{\mathrm{d}t}$$

Where α_v is a fraction of the critical damping coefficient and m_p is the mass of the pellet. α_v is taken equal to 0.9. Further discussion concerning the damping in contacts can be found in [40].

3.5. Numerical sample preparation

Numerical samples are prepared by placing pellets one by one in a rigid cylinder. The initial height of the cylinder, $H_{cell\ 0}$, is set at a value of $H_{cell} + a_{eq\ 0}$, where H_{cell} is the cylinder height during the swelling step. This initial value ensures that all the pellets can be placed in the cylinder. A pellet is placed in the cell each second. The first 20 pellets are randomly placed at the bottom of the cell. Then, each bead is placed at a position corresponding to the lowest elevation in the cell to reproduce experimental preparation (Figure 7a). During this process, the granular assembly is constantly being equilibrated under gravity. When all the pellets are placed in the cell, calculation continues until equilibrium of forces and moments is reached. The cell closure is then simulated by incrementally decreasing the cylinder height from $H_{cell\ 0}$ to H_{cell}. Each height decrease is followed by the calculation of a new equilibrium under gravity before a new decrease. The initial solid fraction of all the numerical samples is the same as in experiment (0.553, corresponding to an inter-pellet porosity of 0.447).

3.6. Equilibrium of forces and moments

At each calculation step, i.e. height decrease during preparation or new suction value during hydration, the granular assembly is considered at equilibrium if both the ratio of the net force F_{net} to the maximum normal force F_{max} and the ratio of the net moment Γ_{net} to the maximum moment Γ_{max} ratio are, on each bead, below a tolerance value ϵ:

(14)
$$|F_{net}| \leq \epsilon\, |F_{max}|$$

(15)
$$|\Gamma_{net}| \leq \epsilon \, |F_{max}| \frac{a_{eq}}{2}$$

ϵ is taken equal to 10^{-4} in all the simulations.

3.7. Swelling pressure calculation

At equilibrium, the swelling pressure P_S^* is computed as the total normal force exerted by the material onto the sensor, divided by the sensor area (Figure 7b). The sensor area is at the centre of the upper wall and defined by the sensor diameter D_{sensor}. Different values of swelling pressure can be calculated from one simulation, depending on the value of D_{sensor}.

4. Results

4.1. Experimental suction-swelling pressure relationship

The evolution of the swelling pressure is measured as a function of elapsed time. Following a change of imposed suction value, the pressure increases or decreases, then reaches a plateau. For each suction value, the plateau value is retained as the corresponding swelling pressure. A new suction value is then imposed (Figure 8a and 8b). Some pressure fluctuations are measured, and are thought to be related to experimental conditions. Room temperature and humidity variations, slight voltage variations in the measurement apparatus, or opening of the bottle containing salt solutions for cleaning (thus temporary modifying the imposed suction), are examples of external perturbations which influence the measurements. Regular cleaning of the bottle was actually compulsory as salt crystallisation on the bottle side would increase the suction, and salt crystallisation inside the tube plunged in the solution would prevent air circulation.

Following the cell closure, SP1 initial pressure was 10 kPa at initial suction 89 MPa. Equilibrium then required ~30; ~120; ~75; ~80; ~35 and ~55 days on imposing 82; 59; 38; 25; 9 and 4 MPa, respectively. Following the cell closure, SP2 initial pressure was 55 kPa. Equilibrium in this test required less time, as an overall plateau value was reached at higher suction, resulting in little pressure variations on imposing new suction values. On imposing 82; 59; 40; 38; 25; 13 and 9 MPa, equilibrium required ~30; ~10; ~20; ~20; ~15; ~25 and ~30 days to be reached, respectively.

The suction-swelling pressure relationships obtained for SP1 and SP2 samples are presented in Figure 9. Results highlighted that upon hydration under constant-volume conditions, the swelling pressure of pellet materials increased in two phases within the considered suction range. The first phase is characterised by an increase of swelling pressure. The second phase is characterised by either a plateau or a decrease of swelling pressure. In SP1 test, the axial pressure ($P_{S\ XP}$) increases from 10 kPa (closure pressure) to 130 kPa when suction is decreased from 89 MPa (initial state) to 25 MPa. $P_{S\ XP}$ slightly increases from 130 kPa to 150 kPa when suction is decreased from 25 MPa to 9 MPa, then slightly decreases to 137 kPa when suction is decreased to 4 MPa. In SP2 test, $P_{S\ XP}$ increases from 55 kPa (closure pressure) to 180 kPa when suction is decreased from 89 MPa to 25 MPa. After this phase, $P_{S\ XP}$ decreases from 180 to 130 kPa when suction is decreased from 25 MPa to 9 MPa.

4.2. Dismantling of experimental samples

SP1 and SP2 isochoric cells were opened after reaching equilibrium at 4 MPa and 9 MPa of suction, respectively. Both SP1 and SP2 samples appeared to be granular. Pellets and macropores could easily be identified (Figure 10a and 10b). Some pellets in contact with the upper wall were deformed in both samples. It was not possible to determine whether it occurred during the closure or during swelling.

4.3. Numerical suction-swelling pressure relationship

Figure 11 presents the results of swelling pressure as a function of suction obtained in simulations DEM1; DEM2 and DEM3. As a reminder, 100 simulations were carried out for DEM1, DEM2, and DEM3. Only the mean values of swelling pressure are plotted, for a ratio of sensor diameter to initial pellet diameter of 4 (as in experimental tests).

In DEM1, the mean value of swelling pressure increases from 0 to 330 kPa as suction decreases from 89 MPa to 60 MPa, then slowly decreases to reach 110 kPa at 4 MPa of suction. In DEM2, swelling pressure reaches 500 kPa during the closure step, then slowly decreases to reach 110 kPa at 4 MPa of suction. In DEM3, the pressure slowly increases to 10 kPa from 89 MPa to 80 MPa of suction, then increases to 250 kPa at 60 MPa of suction, then slowly decreases to 110 kPa as suction decreases to 4 MPa.

4.4. Grain-scale features of numerical samples

4.4.1. Contact plasticity

The evolution of the number of plastic contacts upon hydration is determined in numerical samples. Figures 11a, 11b and 11c present the evolution of the mean plastic contacts proportion for the whole sample, $x^{p}_{c\,tot}$, and for contacts between pellets and the upper wall, where pressure is measured, $x^{p}_{c\,sup}$, for simulations DEM1, DEM2 and DEM3. Results are presented along with the swelling pressure development upon suction decrease. In all samples, the increase in $x^{p}_{c\,sup}$ is more significant than the increase in $x^{p}_{c\,tot}$.

In DEM1, from initial state to 70 MPa of suction, the swelling pressure increases while no contact has reached the elastic limit. The number of plastic contacts increases sharply between 70 MPa and 60 MPa of suction. This suction range corresponds to the peak swelling pressure. The swelling pressure then slowly decreases, as $x^{p}_{c\,sup}$ reaches a maximum and keeps slowly increasing in the whole sample.

The evolution of plastic contacts in DEM3 exhibited a similar trend as in DEM1, but the increase of $x^{p}_{c\,tot}$ and $x^{p}_{c\,sup}$ was not as sharp as in DEM1. In DEM2, the pressure increase due to the cell closure induced contact plasticity. The influence of the closure step in this case is significant. 25 "pellet-upper wall" contacts were created during this step. 15 of these contacts reached the elastic limit during the process, which represents 2.5 % of the overall 600 contacts in the samples. Yet, no significant increase of swelling pressure is recorded upon hydration. The measured pressure keeps decreasing as $x^{p}_{c\,tot}$ and $x^{p}_{c\,sup}$ increase.

4.4.2. Inter-pellet porosity

At initial state, the porosity was ~0.447. Upon pellet swelling, porosity in DEM progressively decreases and reaches a value slightly below 0.2 (Figure 12). This latter is below the minimal value for a dense packing of spheres of same diameter. It highlights that total deflection at contact is non-negligible at low suction. Considering plasticity in contacts allows the elastic deflection, used in equations (8) and (9), to remain small and avoids reaching unrealistically high contact forces.

4.4.3. Coordination number

The coordination number Z, defined by the average number of force-carrying contact per grain, relates to the number of particles N_p, the number of particle-particle contacts $N_{c\,1}$ and the number of particle-wall contacts $N_{c\,2}$ as:

(16)
$$Z = \frac{2\,N_{c\,1} + N_{c\,2}}{N_p}$$

Z is calculated following preparation and upon hydration. Results are presented in Figure 12 for DEM1, DEM2 and DEM3 along with the evolution of inter-pellet porosity.

After closure, the mean coordination number in samples prepared under zero-friction conditions (DEM1 and DEM3) is 5.4. The mean number of contacts in this case is 635, slightly higher than 3 N_p [41], as it should be for frictionless beads approaching the limit of small deflections.

The presence of friction in the assembling stage reduces the number of contacts [40]. Thus samples DEM2 contain 600 contacts on average, with a coordination number of 5.1.

Upon hydration, the coordination number of frictionless samples (DEM3) increases to a final value of 8.2 (net increase: + 2.8). The coordination number of both DEM1 and DEM2 samples increased at the same rate, reaching final values of 7.5 and 7.2 respectively (net increase: + 2.1).

4.4.4. Variability of the results

The coefficient of variation (standard deviation to mean value ratio) of swelling pressure, proportion of plastic contacts and coordination number for the three simulation types is calculated from 100 simulations and presented in Figure 13.

The result variability for swelling pressure and proportion of plastic contacts decreased upon hydration for the three types of simulation. At 9 MPa of suction, its value for swelling pressure reached ~0.10-0.15 (for D_{sensor} / a_{eq} = 4). Its value for proportion of plastic contacts reached ~0.03-0.04. The coefficient of variation of coordination number remained low (< 0.02) for the three types of simulation upon hydration.

4.5. Influence of the sensor diameter

In DEM1, the calculation of swelling pressure from contact forces between pellets and the upper wall is carried out for different values of D_{sensor}. Different suction-swelling pressure relationships are thus obtained. Figure 14 presents the variability of the measured swelling pressure in the 100 DEM1 simulations performed, for two values of the D_{sensor} / $a_{eq\ 0}$ ratio. In both cases, an interval from $m - 2\sigma$ to $m + 2\sigma$ is plotted, with m and σ the mean value and the standard deviation of the swelling pressure, respectively. The mean values are very close for both sensor diameters and are not plotted in Figure 14. The standard deviation significantly increases with decreasing sensor diameter.

The coefficient of variation is determined for six sensor diameter to pellet diameter ratios, at peak measured pressure and at 9 MPa of suction. Results are plotted in Figure 15. The coefficient of variation of the measured swelling pressure reaches 0.8 to 1.3 in the case where both the sensor diameter and the initial pellet diameter are identical.

5. Discussion

The hydromechanical behaviour of expansive clay pellet materials has been studied through swelling pressure tests at laboratory scale and DEM, providing access to grain-scale phenomena. In the following parts, the model validity is first discussed. Then, the material behaviour upon hydration in constant volume conditions as well as interesting contributions of the DEM to interpretation of laboratory tests results and constitutive modelling using double structure models are discussed.

5.1. Model validity

The validity of the modelling approach mainly depends on the following assumptions:

- the material remains granular upon suction decrease;
- the shape of the simulated beads does not induce significant difference of behaviour;
- the contact laws are valid;
- pellet hydration can be simulated by a radius increase.

Sample dismantling allowed the material granular nature to be observed upon hydration to suction value as low as 4 MPa (Figure 10a and 10b). Furthermore, the shape of the pellets was not notably modified. Only local deformation is observable at contact area. These deformations are irreversible.

In the simulations, granules are modelled as isotropic spheres. Their real shape is shown to remain nearly identical upon hydration (Figure 10a and 10b), but is characterised by a cylinder-shaped part between two spherical ends (Figure 1 a and 1 b). Pellets are nonetheless characterised by an aspect ratio (total height to diameter ratio) equal to 1 and considered subspherical. Wiacek et al. (2012) [42] showed that uniaxial compression of subspherical pea seeds could effectively be modelled by spheres in DEM. Furthermore, [36] show small differences between axial and radial values of elastic modulus for pellets within the investigated suction range. It is thus thought that isotropic beads are a suitable choice to model these bentonite pellets.

Assuming linear elasticity, the normal force-deflection relationship at contact is described by the Hertz law (equations (8) and (9)) which had been shown to satisfactorily reproduce the experimental pellet force-deflection relationship [36]. It is proposed to include the influence of grain failure in the model to avoid reaching unrealistically high normal force values. It is assumed that failure initiates at contact and does not depend on the grain stress state. The pellet strength in the granular assembly is thus assumed to be described by the empirical equation proposed for free swelling conditions (equation (4)). As suggested by Figure 10a and 10b, particle failure is more characterised by an irreversible deformation at contact or apparition of cracks than by a general crushing. In this respect, contact plasticity is thought to be an interesting way of modelling this phenomenon as it allows irreversible deflection to arise in simulations. Elastic-plastic contact modelling approach [43, 44] is thus preferred to grain crushing modelling approach [45, 46] to take into account grain failure. Compared to the framework introduced by Thornton and Ning (1998) [43], the granule elastic limit in the present study is given in term of a “limiting contact force”, given by R_A, directly obtained from experimental results [36], instead of a “limiting contact pressure”. Pellet failure in the simulation is thus taken into account by introducing perfect plasticity in the contact law, with the pellet strength decreasing upon hydration (equation (4)). The mean value of the ratio of total deflection to particle diameter using this approach is lower than 0.07.

However, it is worth mentioning that experimental results evidenced a decrease of normal force at failure (constant suction) [36], which is not taken into account by the perfect plasticity of the contact behaviour adopted in the present study. Nevertheless, the calculated swelling pressure for suctions at which most of the contacts had reached the elastic limit appeared to be in the right order of magnitude.

Modelling the swelling of spherical particles within a granular assembly by a radius increase has already been performed in DEM, for super absorbent polymer hydration [35] or thermal expansion effect in granular materials [33, 34]. In these works, a water/heat transfer was introduced and the particles would swell accordingly. In the present work, the approach is slightly different because no transfer law is introduced. All particles swell simultaneously, suction is calculated from equation (3) and all mechanical parameters vary accordingly. It is based on the assumption that vapour diffusion in inter-pellet porosity occurs significantly faster than absorption of water by pellets. The macropores are thought to be full of air at the same relative humidity. From Figure 10a and 10b, it can be observed that the macroporosity is still clearly observable at 4 MPa of suction. In addition, humid air is free to enter the sample macroporosity from either the bottom or the top of the cell (Figure 3). It is thus thought that the suction value imposed to all granules is identical within the isochoric cell. In addition, it is also suggested that there is still free volume available for the pellets to swell.

The model is able to reproduce the general “two phases” trend of the swelling pressure development observed in the laboratory (DEM1 in Figure 9). The first phase, characterised by a sharp increase of swelling pressure until a peak value is reached, is however overestimated by the model. The overestimation of the swelling pressure at high suction in simulation is a consequence of several features: the modelled beads are all identically shaped (perfect spheres of same diameter), cannot rearrange as a consequence of the small cell size (H_{cell} / a_{eq} = 4), and have the same mechanical properties.

It is highlighted in [36] that the variability of pellet mechanical properties is more important at high suction. According to equation (8), the contact force is proportional to the pellet stiffness if all pellets have the same stiffness. In case of a stiffness variability between two pellets in contact, the term E_m / 1 – v^2 in equations (8) would be given by [37]:

(17) $$\frac{E_m}{1-\nu^2} = \frac{1}{\frac{1-\nu_1^2}{E_{m\,1}} + \frac{1-\nu_2^2}{E_{m\,2}}}$$

Where $E_{m\,1}$, $E_{m\,2}$, v_1 and v_2 are the Young modulus of pellet 1 and pellet 2 and the Poisson ratio of pellet 1 and 2 in the contact. Equation (17) highlights that the contact stiffness would be significantly smaller if the Young modulus of one of the pellets in contact were smaller.

The second phase, at lower suction, and lower variability of the mechanical properties, is closer to experimental results. During the second phase, the initial features of the granular assembly have less influence on the macroscopic response because contact forces have reached the elastic limit and the swelling pressure mainly depends on the pellet strength and stiffness decreases upon suction decrease. Thus, swelling pressures in DEM1, DEM2, and DEM3 have comparable values. “Two phases” trends had already been obtained for Febex granular bentonite [19, 30]. In these studies the swelling pressure would increase then remain nearly constant until final saturation (zero suction). It was also suggested that the “plateau” swelling pressure value was a consequence of the pellet strength and stiffness decrease upon hydration.

In the present study, pellet initial diameter is 7 mm. To model pellets of a different size, the simulation method can directly be applied as long as the aforementioned conditions for model validity are verified. Pellet mechanical properties are likely to be influenced by the pellet size [36]. These latter should thus be carefully determined before modelling pellets of different size.

5.2. Limit of the proposed framework at low suction

Wang et al. (2012) [8] proposed an estimation of the final swelling pressure of a compacted bentonite-based material from its initial dry density. From this estimation, the final swelling pressure of the studied material is ~0.21 MPa, higher than the “plateau” value obtained in the swelling pressure tests. The swelling pressure is thus expected to increase upon further suction decrease. Compacted bentonite materials display a change in the hydration and swelling mechanism at low suction. Saiyouri et al. (2004) [47] evidenced that the water uptake mechanisms of compacted MX80 bentonite materials undergo a significant change between ~3 and ~7 MPa of suction. This suction range coincides with a sharp irreversible decrease of the number of layers by clay particle. The proportion of interparticle porosity increases, diffuse double layers are thought to develop and the proportion of interparticle water considerably increases. This is consistent with the transition from the microstructural domain to a dry density-dependent domain of the water retention curve of MX80-based materials [4] and the pore volume reorganisation of MX80 pellets [48].

The DEM model would be unable to reproduce this behaviour and is considered not to be appropriate to describe the swelling pressure evolution upon suction decrease below this threshold (between ~3 and ~7 MPa of suction), even if the material remains granular below these values (Figure 10a and 10b).

5.3. Influence of walls on the measured response

Vargas and McCarthy (2007) [30] performed simulations of particles swelling in both a fixed-walls and a free moving-walls cell. In the first case, particle swelling induced an increase of contact force instead of particle rearrangement. In the second case, the mean contact force was not significantly increasing upon particle radius increase. These two extreme cases highlight that the more particles rearrange, the more the coordination number will increase and the less contact forces will.

The evolution of the mean elastic normal deflection upon radius increase, at contact between pellets and the upper wall, is presented in Figure 16. DEM1 results (optimised preparation and friction during hydration) are characterised by a nearly perfect linear deflection-radius variations relationship until reaching the peak swelling pressure. The linear relationship between these two parameters is close to the “$\Delta\delta_N^e = \Delta R$” line which implies negligible rearrangement of the granular assembly upon swelling. The swelling pressure increase is thus significant and elastic limit in contacts with the upper wall is reached almost simultaneously, resulting in an overestimated peak value and an accentuated transition between phases 1 and 2. This tendency towards deflection increase instead of particle rearrangement in the simulations is also underlined in Figure 16 by the significant increase of the mean elastic normal deflection after the cell closure in DEM2 (friction during preparation). The considered solid fraction (0.553) is low and these features should not be observed in larger granular assemblies, less influenced by walls. Since pellet-wall contacts are stiffer than pellet-pellet contacts, negligible rearrangements also explain the more significant increase in contact plasticity at contact with walls compared to the mean increase in the samples. As a consequence, the post-peak decrease of swelling pressure can be overestimated if swelling pressure is measured at contact with the wall instead of calculating the mean stress in the sample (Figure 17).

The influence of the walls is furthermore underlined by the coordination number following preparation (Figure 12): the coordination number of frictionless bead assemblies was 5.4 instead of the bulk value ~6 [41].

These results suggest that the variability associated to sample preparation stems from wall influence. Experimental tests are influenced by the walls as well, because they share the same solid fraction and H_{cell} / $a_{eq\ 0}$ ratio.

5.4. Contribution of DEM to laboratory testing

Thanks to the DEM ability to model the wall-pellet interaction and access grain-scale phenomena, simulation results can provide an insight into swelling pressure tests carried out at laboratory scale, especially since walls have non-negligible influence on the measured response.

The influence of sample preparation on test results was highlighted by DEM simulations (Figure 9). The general trend of DEM2 results suggests that initial pressure required to close the cell before hydration can cause a significant increase of plastic contact proportion (Figure 11b). As a consequence, hydration phase 1 appeared very limited in DEM2. The sample behaviour was mainly controlled by equations (2) and (4) and the number of contacts between pellets and the upper wall, rather than the particle swelling. Even if plasticity does not arise during the closure step, closure can have an influence on the behaviour upon hydration. At granular state, the mean stress in the sample is proportional to the product of coordination number and mean contact force. It was highlighted in Figure 12 that the evolution of the coordination number was not influenced by the sample preparation. Thus, samples prepared under higher initial closure pressure are likely to reach plasticity more rapidly. This is actually suggested by SP1 and SP2 test results. It is recommended that the control of the initial state is as important as the value of the sample density to study the swelling pressure development of pellet materials.

Beside variability arising from wall influence, small pressure sensors in the laboratory have been shown to induce additional variability of the measured swelling pressure. DEM allowed the influence of the pressure sensor diameter on the variability of the measured swelling pressure to be quantified. This variability, along with the variability of behaviour associated to the sample small size, increases the difficulty to study the intrinsic behaviour of pellet mixtures at laboratory scale. For granules with the same mechanical behaviour, the coefficient of variation of swelling pressure obtained from simulations thus depends on both the preparation in a small cell and the ratio of sensor diameter to pellet diameter.

It was discussed that an overestimation of the calculated swelling pressure can arise in the elastic phase of the granule swelling from some of the model simplifications, especially at the highest suction values. However, concerning the variability of this measure, these simplifications can reduce the coefficient of variation. Owing to the dispersion of the granule real mechanical properties at high suctions, the calculated coefficient of variation associated to swelling pressure is likely to be underestimated by the model in the elastic part of the hydration path. As contact forces reach the elastic limit, normal forces reach less dispersed values and the calculated coefficient of variation decreases.

These results are of importance, since most of the time the material behaviour is studied at laboratory scale, with inevitable constraints concerning the number and sizes of sensors, related to the cell size. It is recommended that experiments performed to determine material parameters for modelling purpose should be interpreted carefully considering the order of magnitude of the variability.

Simulation results highlighted the influence of interactions at contacts between pellets on the material behaviour upon hydration. Since pellets would lose their structure upon full saturation, the material behaviour is sensitive to the hydration method at laboratory scale. The influence of the granular nature of the material is likely to be underestimated upon fast liquid water hydration.

5.5. Contribution of DEM to constitutive modelling of pellet materials

The proposed DEM model has been shown to reproduce the main features of the material behaviour upon partial hydration in constant-volume conditions. The relationships between the behaviour of the granules and the macrostructural behaviour can be identified. It can provide valuable information for the modelling of pellet mixture behaviour using double structure models. This modelling framework has been used in previous studies to model pellet materials upon hydration, considering the pellet phase as the microstructure [20, 21, 23].

For this purpose, DEM can be a complementary tool to experimental studies. It was highlighted that results of experimental tests performed at the laboratory scale on pellet mixtures can be characterised by a significant variability. This latter can make the determination of the material intrinsic behaviour difficult. DEM allows uncertainty and variability to be taken into account, at low simulation cost. DEM model parameters can be determined from experimental tests at the pellet scale [36]. Then, the model can be validated against swelling pressure tests or other common tests at the laboratory scale.

Simulations may be performed in conditions where the intrinsic behaviour of the material can be addressed. DEM could help determining constitutive laws for the mechanical behaviour of a pellet assembly and relationship between pellet swelling and pellet assembly swelling. In this respect, a perspective arising from the present study results is to perform DEM simulations of large pellet assemblies of different solid fractions upon hydration, avoiding the influence of wall and small sample sizes. In this way, constitutive laws describing the material before homogenisation could be proposed and integrated in a double structure model.

6. Conclusions

The hydromechanical behaviour of pellet assemblies was studied through laboratory and DEM-simulated swelling pressure tests. DEM model parameters were obtained from pellet scale experimental characterisation. The DEM model was validated against experimental results. Numerical results allowed the experimental results to be interpreted with respect to grain scale phenomena.

Compared to traditional compacted powder materials, pellet materials are characterised by an initial granular nature, which was shown in the present study to control the material behaviour upon hydration to suction as low as 4 MPa. In particular, it was shown that, in constant volume conditions, the granule strength and stiffness control the macroscopic response. Upon hydration, the swelling pressure develops in two phases. The first is characterised by an elastic increase of the normal contact forces and is affected by the initial state of the material, thus the sample preparation in laboratory tests. The second is characterised by the occurrence of contact plasticity and is less affected by the initial state.

DEM simulations satisfactorily reproduced the material behaviour observed at laboratory scale. DEM results suggest that the 30 mm x 60 mm isochoric cell (H_{cell} / $a_{eq\ 0}$ = 4) was not a true representative elementary volume, due to its small size and the significant influence of the walls. In addition, it was shown that a low value of the ratio of sensor diameter to pellet diameter induces significant measurement variability in the investigated suction range.

A perspective arising from the present study is the DEM modelling of large pellet assemblies upon hydration, with no influence of the walls. Constitutive laws for the material before homogenisation could be proposed and provide an interesting framework for further FEM simulations of the entire hydration path, using double structure models in which pellets could be considered as the microstructural phase.

Conflict of Interest:

The authors declare that they have no conflict of interest.

References

1. Blatz JA, Graham J, Chandler NA (2002) Influence of suction on the strength and stiffness of compacted sand–bentonite. Can Geotech J 39:1005–1015. https://doi.org/10.1139/t02-056
2. Lloret A, Villar M V, Sanchez M, et al (2003) Mechanical behaviour of heavily compacted bentonite under high suction changes. Geotechnique 53:27–40. https://doi.org/10.1680/geot.53.1.27.37258
3. Agus SS, Schanz T (2005) Effect of Shrinking and Swelling on Microstructures and Fabric of a Compacted Bentonite-Sand Mixture. Proc Int Conf Probl Soils, 25-27 May 2005, East Mediterr Univ Famagusta, N Cyprus

4. Villar M V. (2007) Water retention of two natural compacted bentonites. Clays Clay Miner 55:311–322. https://doi.org/10.1346/CCMN.2007.0550307

5. Saiyouri N, Hicher PY, Tessier D (2000) Microstructural approach and transfer water modelling in highly compacted unsaturated swelling clays. Mech Cohesive-frictional Mater 5:41–60

6. Delage P, Marcial D, Ruiz X, Cui YJ (2006) Ageing effects in a compacted bentonite: a microstructure approach. Géotechnique 56:291–304. https://doi.org/10.1680/geot.2006.56.5.291

7. Tang, AM, Cui YJ, Le TT (2008) A study on the thermal conductivity of compacted bentonites. Appl Clay Sci 41:181–189

8. Wang Q, Tang AM, Cui YJ, et al (2012) Experimental study on the swelling behaviour of bentonite/claystone mixture. Eng Geol 124:59–66. https://doi.org/10.1016/j.enggeo.2011.10.003

9. Saba S, Cui Y, Tang AM, Barnichon J (2014) Investigation of the swelling behaviour of compacted bentonite-sand mixtures by mock-up tests. Can Geotech J 51:1399–1412

10. Sun H, Mašín D, Najser J, et al (2019) Bentonite microstructure and saturation evolution in wetting-drying cycles evaluated using ESEM, MIP and WRC measurements. Geotechnique 69:713–726. https://doi.org/10.1680/jgeot.17.P.253

11. Seiphoori A, Ferrari A, Laloui L (2014) Water retention behaviour and microstructural evolution of MX-80 bentonite during wetting and drying cycles. Géotechnique 64:721–734. https://doi.org/10.1680/geot.14.P.017

12. Massat L, Cuisinier O, Bihannic I, et al (2016) Swelling pressure development and inter-aggregate porosity evolution upon hydration of a compacted swelling clay. Appl Clay Sci 124–125:197–210. https://doi.org/10.1016/j.clay.2016.01.002

13. Keller LM, Seiphoori A, Gasser P, et al (2014) The pore structure of compacted and partly saturated MX-80 bentonite at different dry densities. Clays Clay Miner 62:174–187. https://doi.org/10.1346/CCMN.2014.0620302

14. Komine H, Ogata N (2003) New equations for swelling characteristics of bentonite-based buffer materials. Can Geotech J 40:460–475. https://doi.org/10.1139/t02-115

15. Cuisinier O, Masrouri F (2005) Hydromechanical behaviour of a compacted swelling soil over a wide suction range. Eng Geol 81:204–212. https://doi.org/10.1016/j.enggeo.2005.06.008

16. Karnland O, Nilsson U, Weber H, Wersin P (2008) Sealing ability of Wyoming bentonite pellets foreseen as buffer material - Laboratory results. Phys Chem Earth 33:472–475. https://doi.org/10.1016/j.pce.2008.10.024

17. Volckaert, G., Bernier, F., Alonso, E. E., et al (1996). Thermal-hydraulic-mechanical and geochemical behaviour of the clay barrier in radioactive waste repositories (model development and validation), EUR 16744 EN. Luxembourg: Publications of the European Communities.

18. van Geet M, Volckaert G, Roels S (2005) The use of microfocus X-ray computed tomography in characterising the hydration of a clay pellet/powder mixture. Appl Clay Sci 29:73–87. https://doi.org/10.1016/j.clay.2004.12.007

19. Hoffmann C, Alonso EE, Romero E (2007) Hydro-mechanical behaviour of bentonite pellet mixtures. Phys Chem Earth 32:832–849. https://doi.org/10.1016/j.pce.2006.04.037

20. Alonso EE, Romero E, Hoffmann C (2011) Hydromechanical behaviour of compacted granular expansive mixtures: experimental and constitutive study. Géotechnique 61:329–344. https://doi.org/10.1680/geot.2011.61.4.329

21. Gens A, Valleján B, Sánchez M, et al (2011) Hydromechanical behaviour of a heterogeneous compacted soil: experimental observations and modelling. Géotechnique 61:367–386. https://doi.org/10.1680/geot.SIP11.P.015

22. Molinero-Guerra A, Mokni N, Delage P, et al (2017) In-depth characterisation of a mixture composed of powder/pellets MX80 bentonite. Appl Clay Sci 135:538–546. https://doi.org/10.1016/j.clay.2016.10.030

23. Mokni N, Molinero-Guerra A, Cui Y-J, et al (2019) Modelling the long-term hydro-mechanical behaviour of a bentonite pellet/powder mixture with consideration of initial structural heterogeneities. Géotechnique 1–61. https://doi.org/10.1680/jgeot.18.p.110

24. Zhang Z, Ye W, Liu Z, et al (2020) Mechanical behavior of GMZ bentonite pellet mixtures over a wide suction range. Eng Geol 264:105383. https://doi.org/10.1016/j.enggeo.2019.105383

25. Liu Z, Ye W, Zhang Z, et al (2019) Particle size ratio and distribution effects on packing behaviour of crushed GMZ bentonite pellets. Powder Technol 351:92–101. https://doi.org/10.1016/j.powtec.2019.03.038

26. Liu, Z., Cui, Y., Ye, W. et al (2020) Investigation of the hydro-mechanical behaviour of GMZ bentonite pellet mixtures. Acta Geotech. https://doi.org/10.1007/s11440-020-00976-y

27. Molinero-Guerra A, Aimedieu P, Bornert M, et al (2018) Analysis of the structural changes of a pellet/powder bentonite mixture upon wetting by X-ray computed microtomography. Appl Clay Sci 165:164–169. https://doi.org/10.1016/j.clay.2018.07.043

28. Yigzaw ZG, Cuisinier O, Massat L, Masrouri F (2016) Role of different suction components on swelling behavior of compacted bentonites. Appl Clay Sci 120:81–90. https://doi.org/10.1016/j.clay.2015.11.022

29. Imbert C, Villar MV (2006) Hydro-mechanical response of a bentonite pellets/powder mixture upon infiltration. Appl Clay Sci 32:197–209. https://doi.org/10.1016/j.clay.2006.01.005

30. Molinero Guerra A, Cui YJ, Mokni N, et al (2018) Investigation of the hydro-mechanical behaviour of a pellet/powder MX80 bentonite mixture using an infiltration column. Eng Geol 243:18–25. https://doi.org/10.1016/j.enggeo.2018.06.006

31. Alonso EE, Hoffmann C, Romero E (2010) Pellet mixtures in isolation barriers. J Rock Mech Geotech Eng 2:12–31. https://doi.org/10.3724/SP.J.1235.2010.00012

32. Radjai, F. & Dubois, F. (2011). Discrete-element modeling of granular materials. Wiley-ISTE, ISBN 978-1-84821-260-2.

33. Vargas WL, McCarthy JJ (2007) Thermal expansion effects and heat conduction in granular materials. Phys Rev E - Stat Nonlinear, Soft Matter Phys 76:1–8. https://doi.org/10.1103/PhysRevE.76.041301

34. Zhao S, Evans TM, Zhou X, Zhou S (2017) Discrete element method investigation on thermally-induced shakedown of granular materials. Granul Matter 19:1–11. https://doi.org/10.1007/s10035-016-0690-5

35. Sweijen T, Chareyre B, Hassanizadeh SM, Karadimitriou NK (2017) Grain-scale modelling of swelling granular materials; application to super absorbent polymers. Powder Technol 318:411–422. https://doi.org/10.1016/j.powtec.2017.06.015

36. Darde B, Tang AM, Pereira J-M, et al (2018) Hydro-mechanical behaviour of high-density bentonite pellet on partial hydration. Géotechnique Lett 8:330–335. https://doi.org/10.1680/jgele.18.00114

37. Johnson KL (1985) Contact Mechanics. Cambridge University Press, Cambridge, UK

38. Darde B, Tang AM, Roux JN, et al (2020) Effects of the initial granular structure of clay sealing materials on their swelling properties : experiments and DEM simulations. EPJ Nuclear Sci. Technol. 6. https://doi.org/10.1051/epjn/2019059.

39. Tang A-M, Cui Y-J (2005) Controlling suction by the vapour equilibrium technique at different temperatures and its application in determining the water retention properties of MX80 clay. Can Geotech J 42:287–296. https://doi.org/10.1139/t04-082

40. Agnolin I, Roux JN (2007) Internal states of model isotropic granular packings. I. Assembling process, geometry, and contact networks. Phys Rev E - Stat Nonlinear, Soft Matter Phys 76:1–27. https://doi.org/10.1103/PhysRevE.76.061302

41. Roux J-N (2000) Geometric origin of mechanical properties of granular materials. Phys Rev E - Stat Nonlinear, Soft Matter Phys 61:1–35

42. Wiacek J, Molenda M, Horabik J, Ooi JY (2012) Influence of grain shape and intergranular friction on material behavior in uniaxial compression: Experimental and DEM modeling. Powder Technol 217:435–442. https://doi.org/10.1016/j.powtec.2011.10.060

43. Thornton C, Ning Z (1998) A theoretical model for the stick/bounce behaviour of adhesive, elastic- plastic spheres. Powder Technol 99:154–162. https://doi.org/10.1016/S0032-5910(98)00099-0

44. Thornton C, Cummins SJ, Cleary PW (2017) On elastic-plastic normal contact force models, with and without adhesion. Powder Technol 315:339–346. https://doi.org/10.1016/j.powtec.2017.04.008

45. Bolton MD, Nakata Y, Cheng YP (2008) Micro- and macro-mechanical behaviour of DEM crushable materials. Géotechnique 58:471–480. https://doi.org/10.1680/geot.2008.58.6.471

46. Cheng YP, Bolton MD, Nakata Y (2004) Crushing and plastic deformation of soils simulated using DEM. Géotechnique 54:131–141. https://doi.org/10.1680/geot.2004.54.2.131

47. Saiyouri N, Tessier D, Hicher PY (2004) Experimental study of swelling in unsaturated compacted clays. Clay Miner 39:469–479. https://doi.org/10.1180/0009855043940148

48. Molinero-Guerra A, Delage P, Cui Y-J, et al (2019) Water retention properties and microstructure changes of a bentonite pellet upon wetting/drying; application to radioactive waste disposal. Géotechnique 1–41. https://doi.org/10.1680/jgeot.17.p.291

List of symbols

$a_{eq\ 0}$: initial sphere diameter in the simulations

$a_{eq\ i}$: sphere diameter at step i in the simulations

a_{eq}: sphere diameter in the simulations

C_A: model parameter

D_0: initial diameter of the pellet

D_{sensor}: diameter of the pressure sensor

E_m: pellet Young modulus

F_{max}: maximum normal force on a particle

F_N: normal contact elastic force

F_{net}: net force on a particle

F_T: norm of the tangential reaction vector

$\boldsymbol{F_T}$: tangential reaction vector

$\dot{\boldsymbol{F}}_{\boldsymbol{T}}$: increment of tangential reaction vector

h_0: initial height of the cylinder-shaped part of the pellet

H_0: initial total height of the pellet

H_{cell} 0: initial height of the cylinder

H_{cell}: height of the cylinder during the swelling step

m: mean value

m_p: mass of the pellet

$N_{c\ 1}$: number of particle-particle contacts

$N_{c\ 2}$: number of particle-wall contacts

N_p: number of particles

N^v: viscous component of the contact force

p': effective mean stress

P_S^*: apparent swelling pressure at equilibrium in the simulations

$P_{S\ XP}$: axial pressure in swelling pressure tests

R_A: pellet strength

R_c: curvature radius of the pellet

s_0: initial suction of the pellet

V: volume of the pellet

w_0: initial water content of the pellet

$x_{c\,sup}^{p}$: evolution of the mean plastic contacts proportion for contacts between pellets and the upper wall

$x_{c\,tot}^{p}$: evolution of the mean plastic contacts proportion for the whole sample

Z: coordination number

α_m: model parameter

α_v: Damping parameter

β_m: model parameter

Γ_{max}: maximum moment on a particle

Γ_{net}: net moment on a particle

δ_N^e: normal elastic deflection at contact

$\Delta\delta_N^e$: variation of the mean normal elastic deflection during particle swelling

ΔR: variation of the particle radius during swelling

$\boldsymbol{\delta_T}$: relative tangential displacement vector

$\dot{\boldsymbol{\delta}}_{\boldsymbol{T}}$: increment of relative tangential displacement vector

ϵ: tolerance value for equilibrium in the simulations

λ_i: parameter describing the diameter increment at step i in DEM

λ_0: parameter describing the diameter increment at initial state in DEM

λ_f: parameter describing the diameter increment at final state in DEM

ε_{Vm}: pellet volumetric strain

μ: friction coefficient

v: pellet Poisson ratio

ρ_{d0}: initial dry density of the pellet

ρ_s: MX80 particle density

σ: standard deviation

TABLES AND TABLE CAPTIONS

TABLE 1 Properties of the MX80 bentonite

Property	Value
Particle density, ρ_s (g/cm^3)	2.77
Smectite content (%)	80
Liquid limit (%)	560
Plastic limit	53
CEC (meq/g)	98/100

TABLE 2 Initial properties of the granules

Property	Value
Dry density, ρ_{d0} (Mg/m^3)	1.90
Water content, w_0 (%)	12.2
Diameter, D_0 (mm)	7.0
Height, H_0 (mm)	7.0
Height of the cylinder-shaped part, h_0 (mm)	5.0
Curvature radius, R_c (mm)	6.5
Suction, s_0 (MPa)	89

TABLE 3 Geometrical properties of isochoric cells

Property	Value
Sample height, H_{cell} (mm)	30
Sample diameter, D_{cell} (mm)	60
Sensor diameter, D_{sensor} (mm)	30
Sample volume (mm^3)	84823

TABLE 4 Suction values imposed using the vapour equilibrium technique

Salt solution	Suction (MPa)
$Mg(NO3)_2$	82
NH4NO3	59
NaNO3	40
NaCl	38
$(NH4)_{2SO4}$	25
Na2CO3	13
KNO3	9
K2SO4	4

TABLE 5 Friction values used during preparation and hydration steps in DEM1, DEM2 and DEM3 simulations. 100 simulations are performed for each type of simulation

Simulation	μ (preparation step) (-)	μ (swelling step) (-)
DEM01	0	0.3
DEM02	0.3	0.3
DEM03	0	0

FIGURES AND FIGURE CAPTIONS

Fig. 1 Schematic view of a pellet

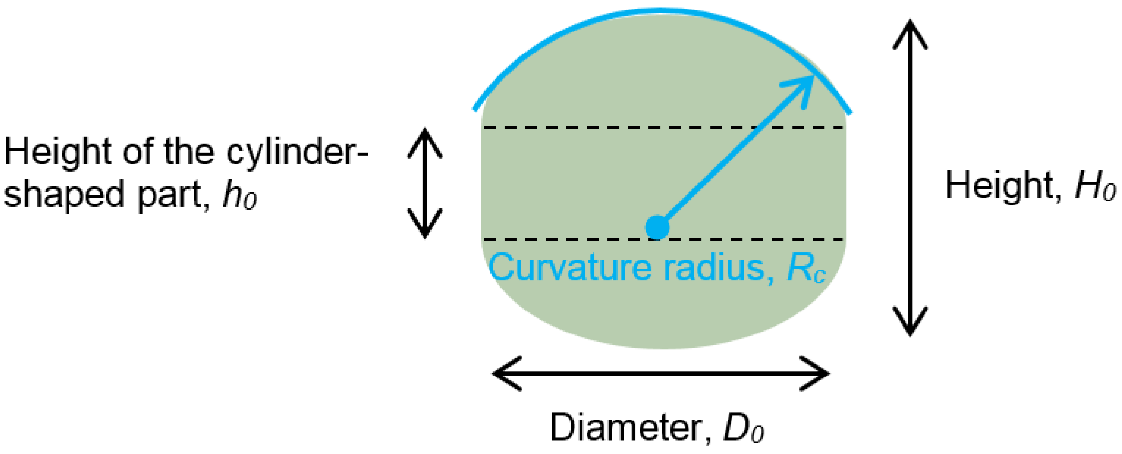

Fig. 2 Isochoric cell used for swelling pressure tests

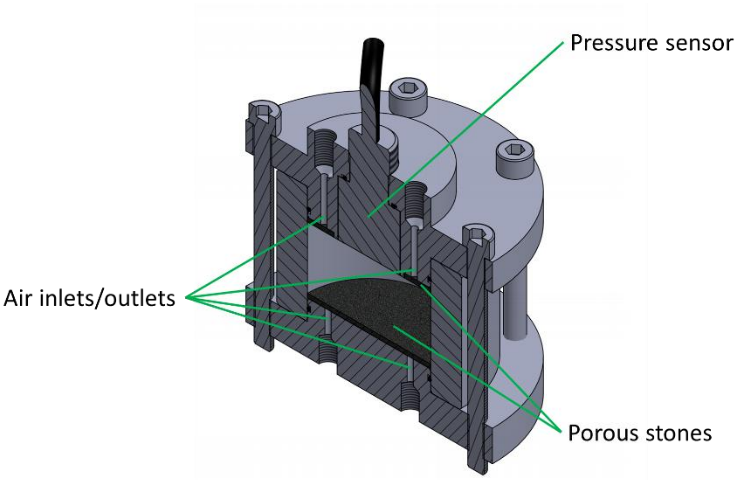

Fig. 3 Air circulation in the isochoric cell

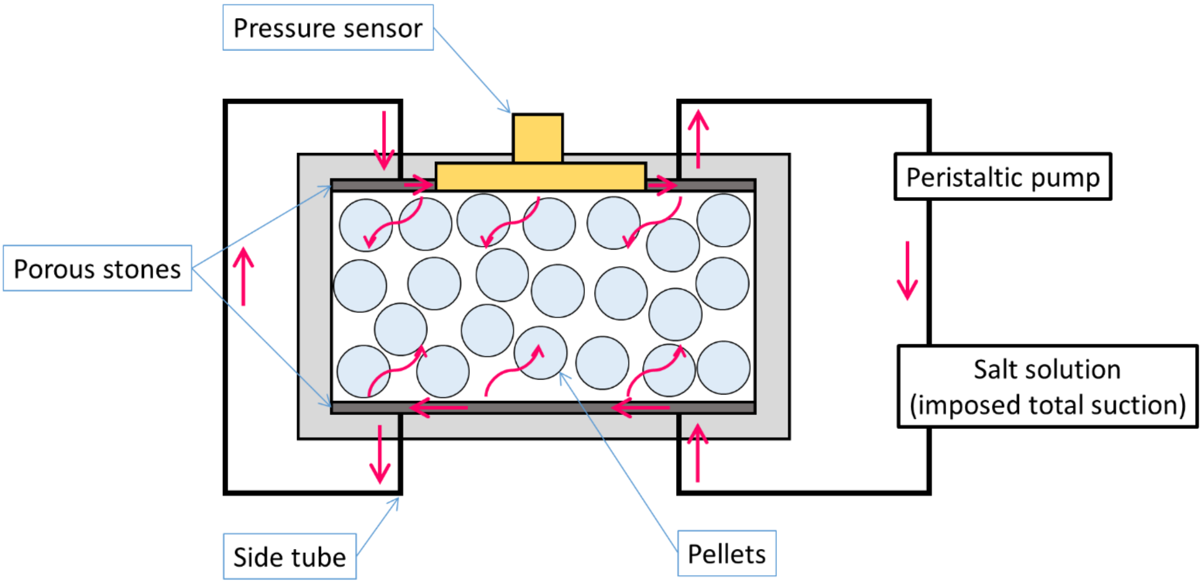

Fig. 4a Hydromechanical behaviour of a pellet (Darde et al., 2018). a) Evolution of Volumetric strain upon suction decrease for one pellet

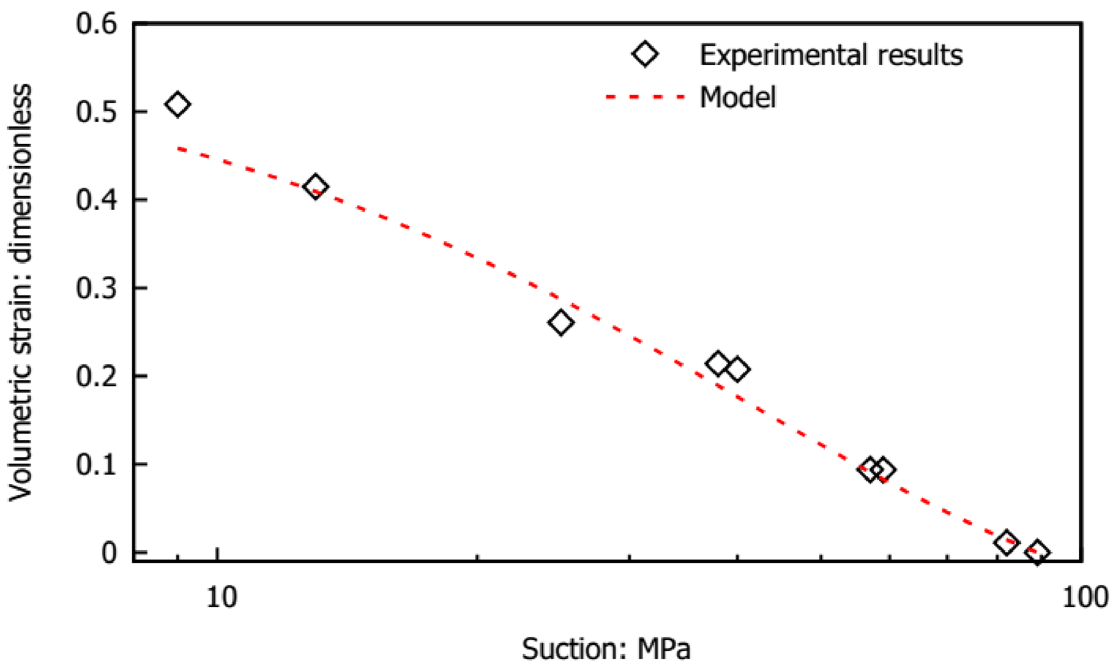

Fig. 4b Evolution of Modulus and Strength upon suction decrease for one pellet

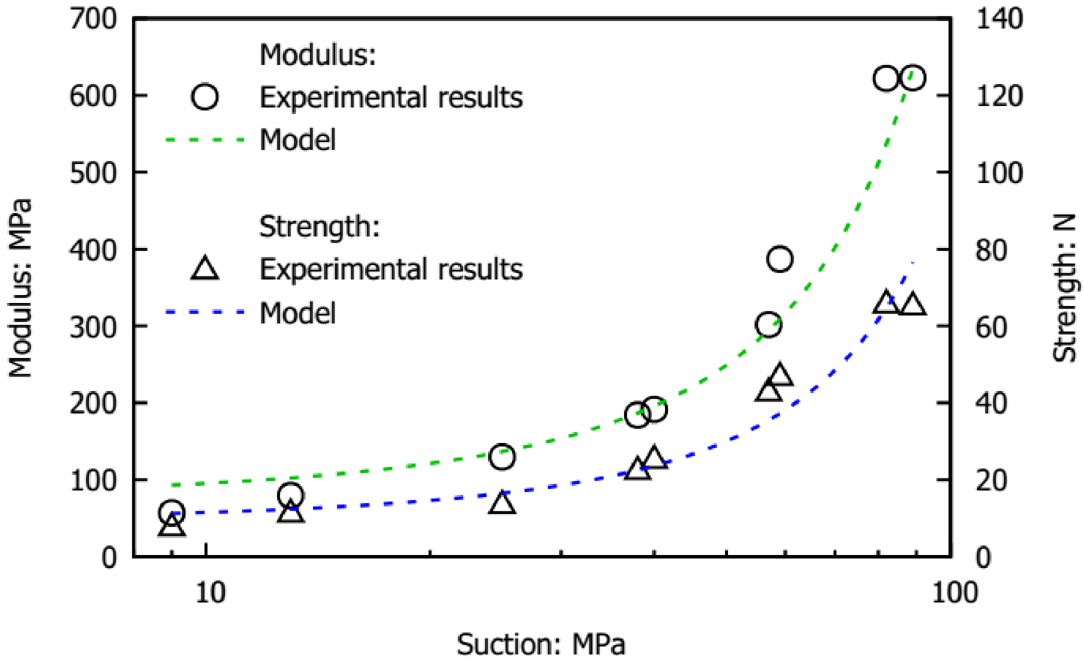

Fig. 5 Contact between two particles in DEM

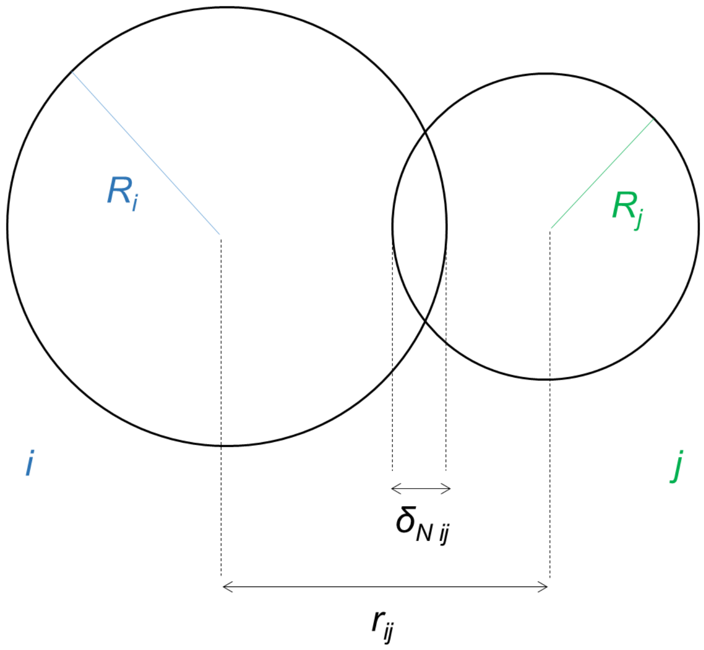

Fig. 6a Contact laws used in the model: Normal reaction: Hertz law + perfect plasticity

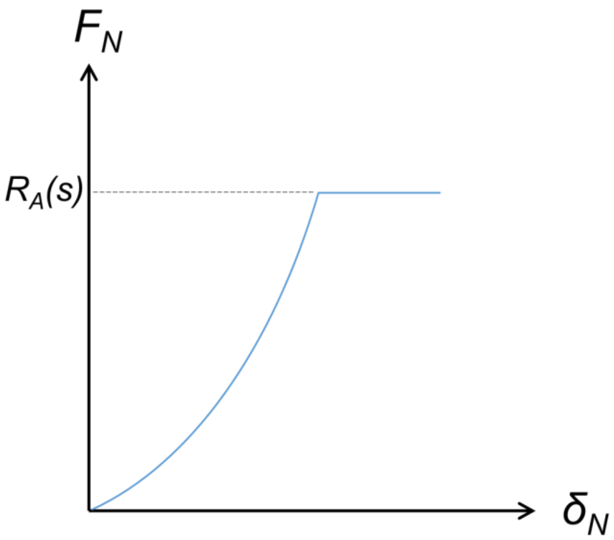

Fig 6b Tangential reaction: Simplified elasticity law + Coulomb friction

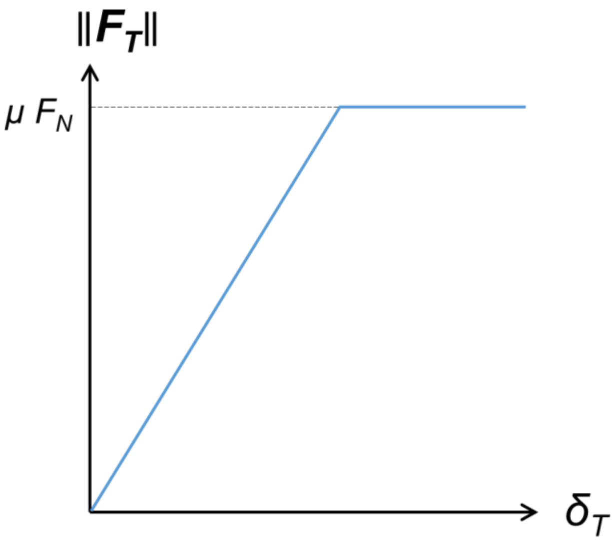

Fig. 7a Preparation step in DEM

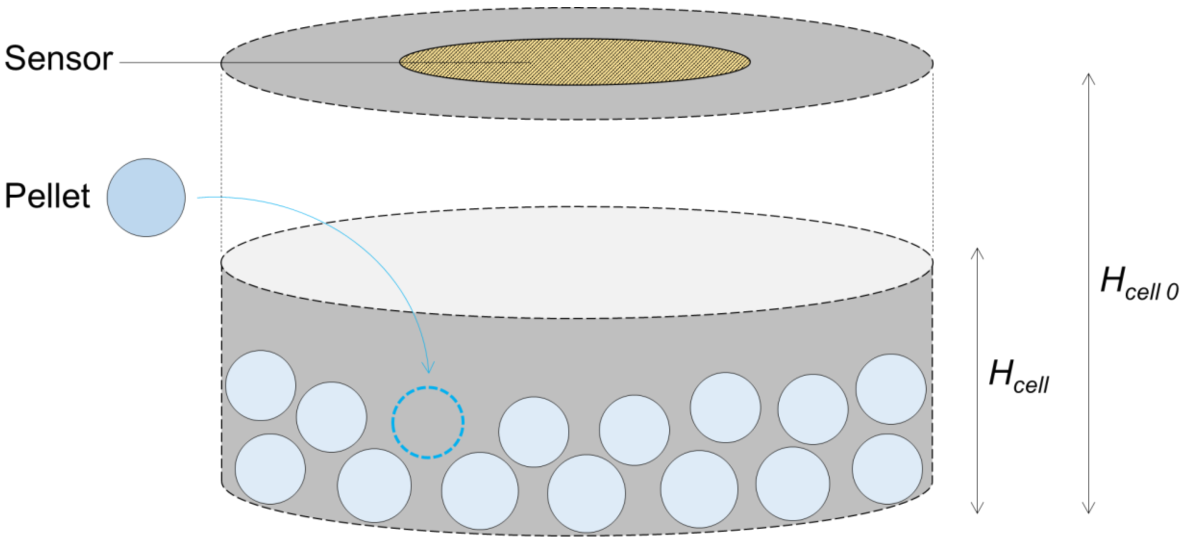

Fig. 7b Dimensions of the isochoric cell

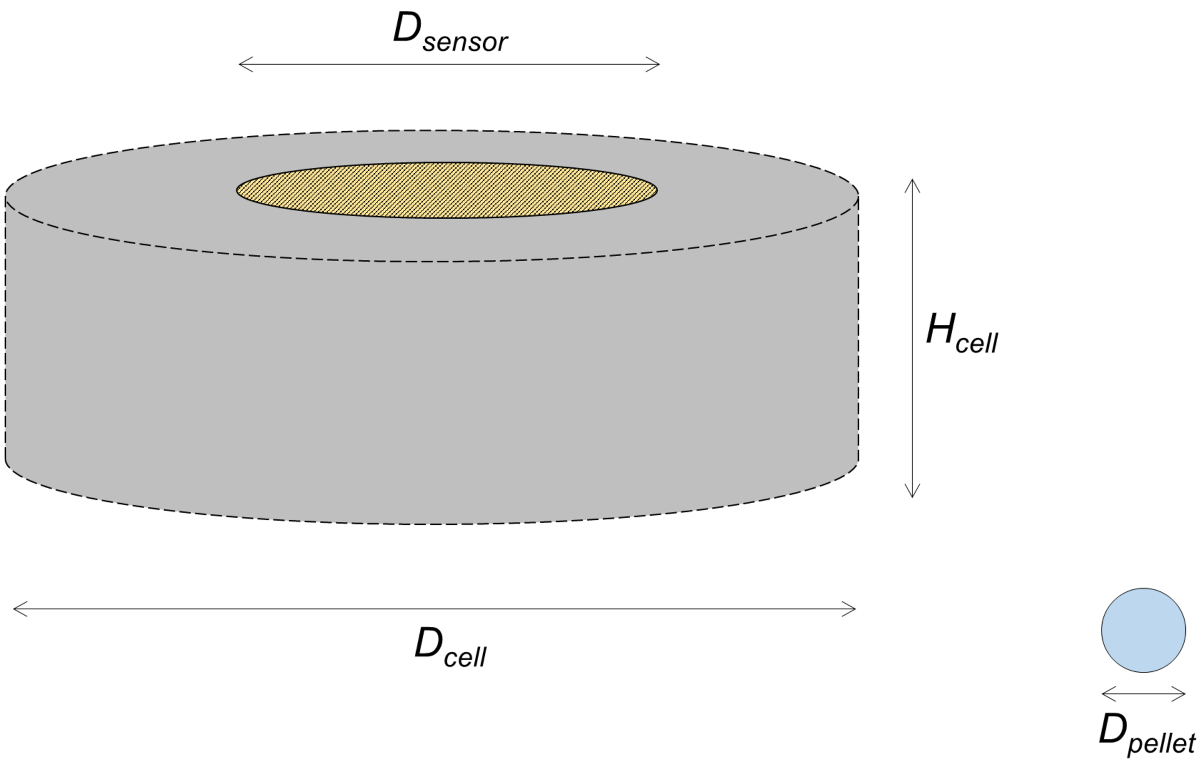

Fig. 8a Swelling pressure as a function of elapsed time for SP1

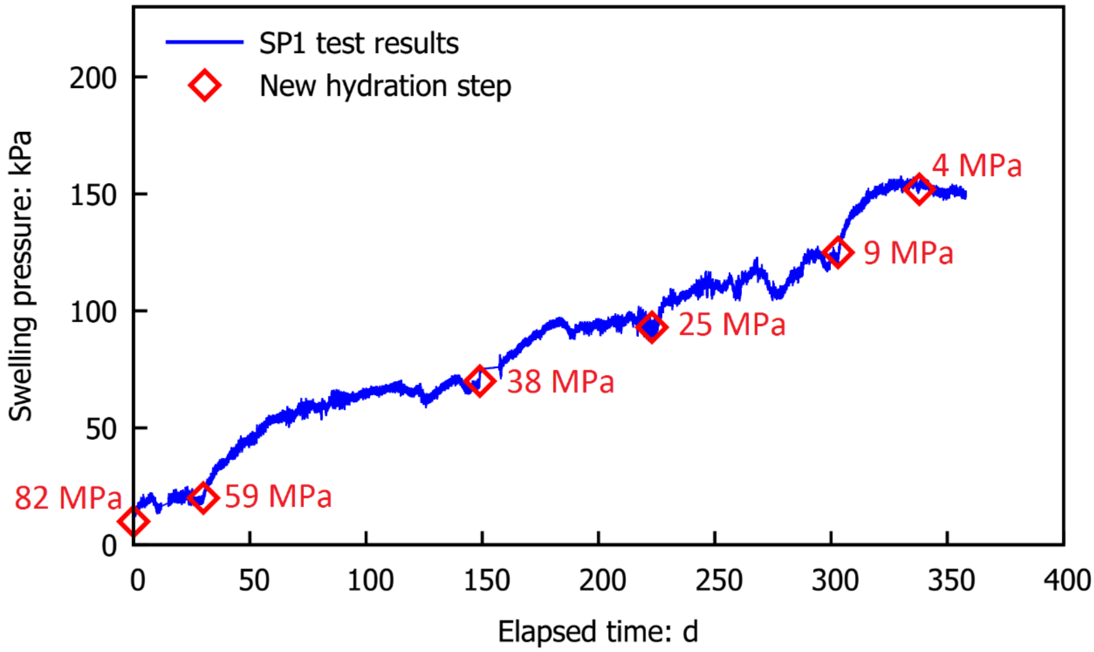

Fig. 8b Swelling pressure as a function of elapsed time for SP2

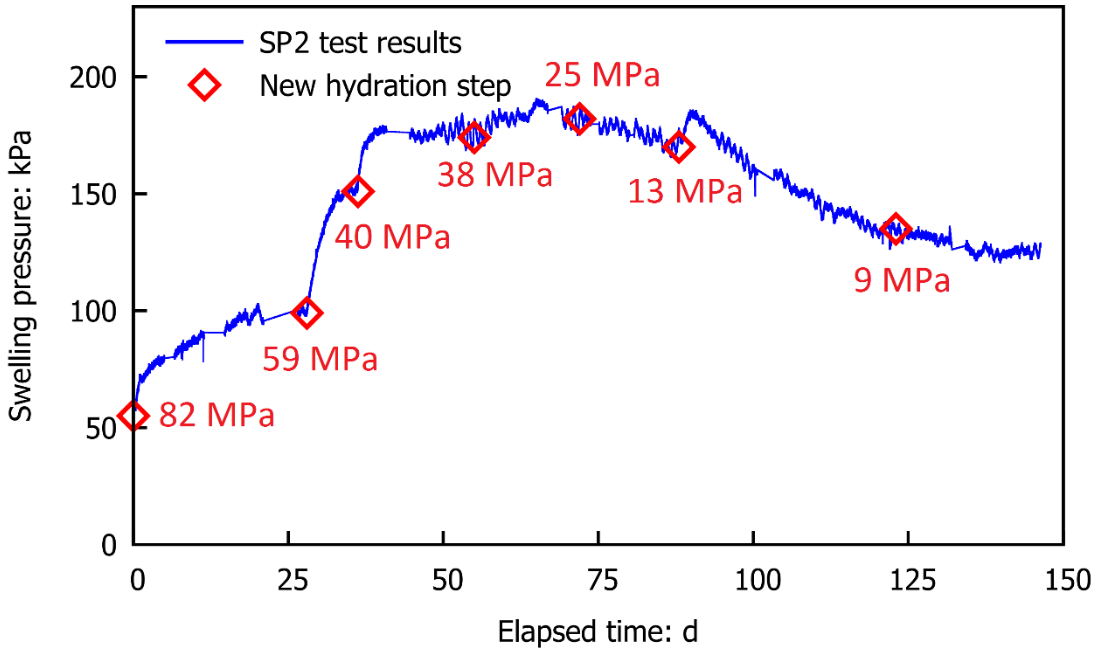

Fig. 9 Swelling pressure as a function of decreasing suction for SP1 and SP2, along with the mean value obtained for DEM1, DEM2 and DEM3 simulations.

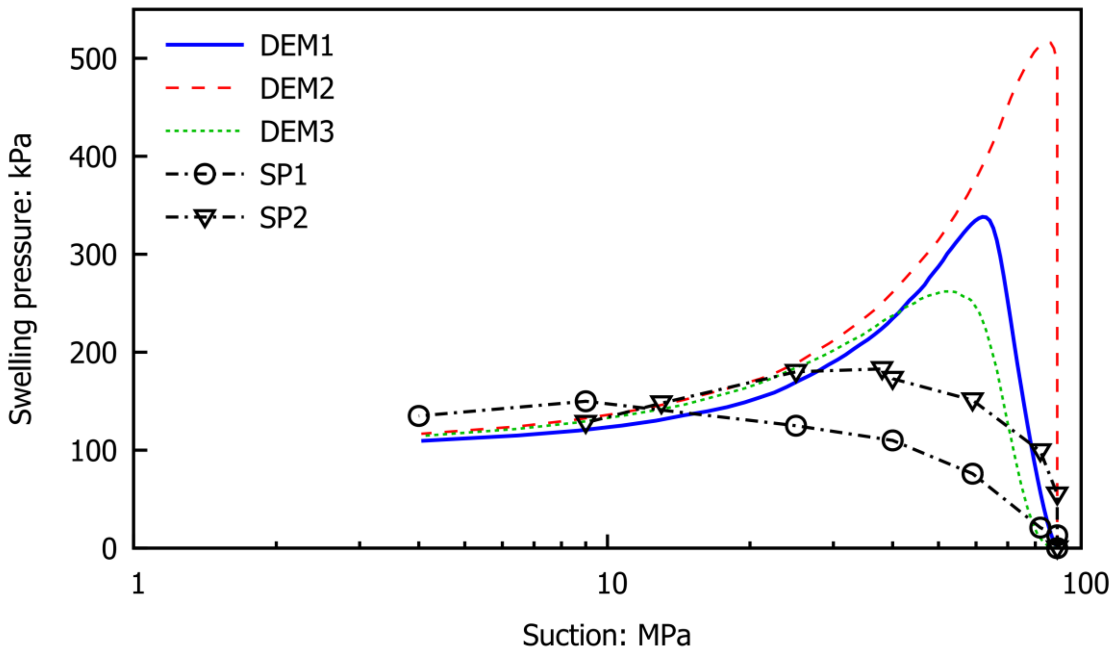

Fig. 10a Picture of the SP1 sample after dismantling at 4 MPa of suction. The cell diameter is 60 mm

Fig. 10b Picture of the SP2 sample after dismantling at 9 MPa of suction. The cell diameter is 60 mm

Fig. 11a Mean value of swelling pressure, proportion of plastic contacts in the sample and proportion of plastic contacts at the top wall in DEM1

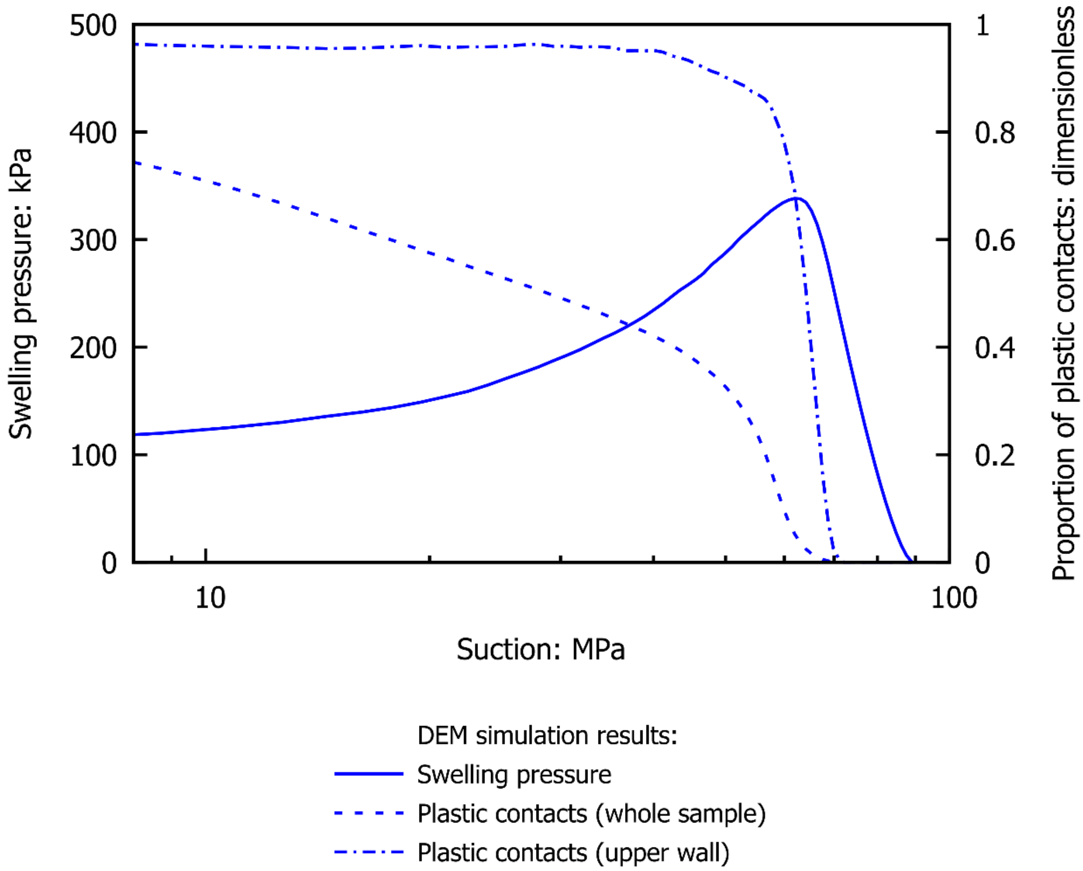

Fig. 11b Mean value of swelling pressure, proportion of plastic contacts in the sample and proportion of plastic contacts at the top wall in DEM2

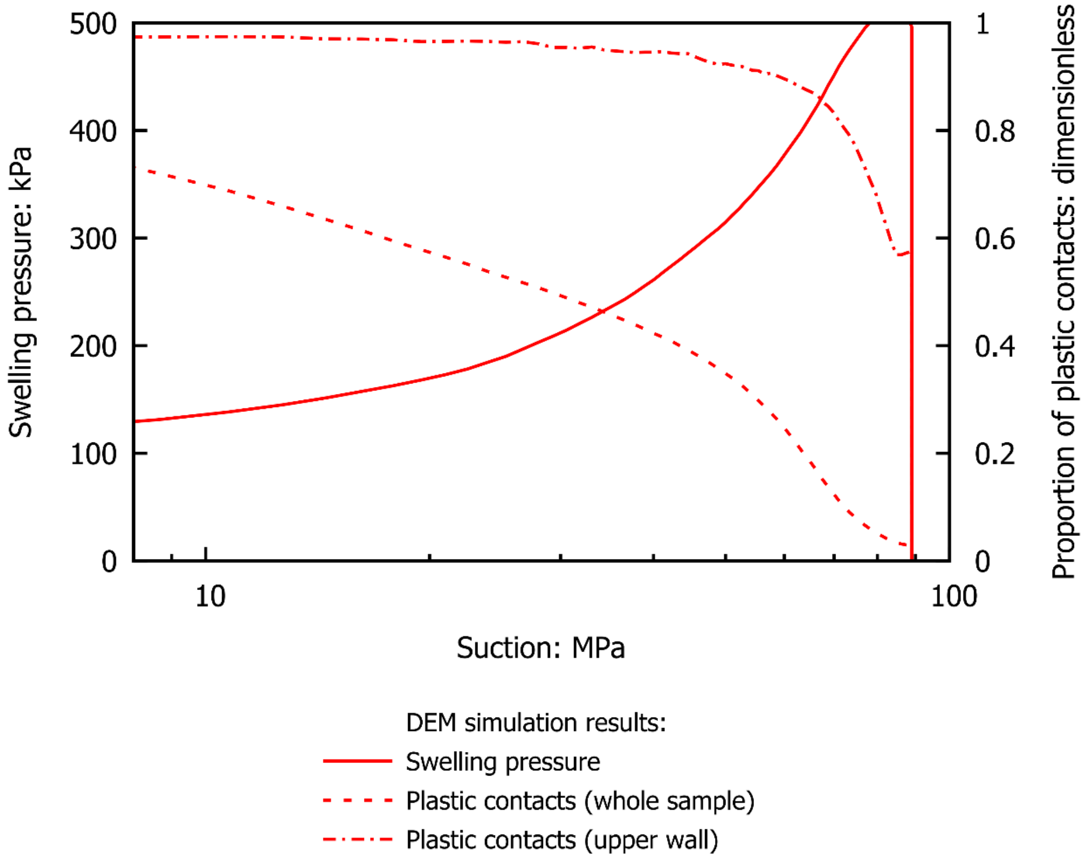

Fig. 11c Mean value of swelling pressure, proportion of plastic contacts in the sample and proportion of plastic contacts at the top wall in DEM3

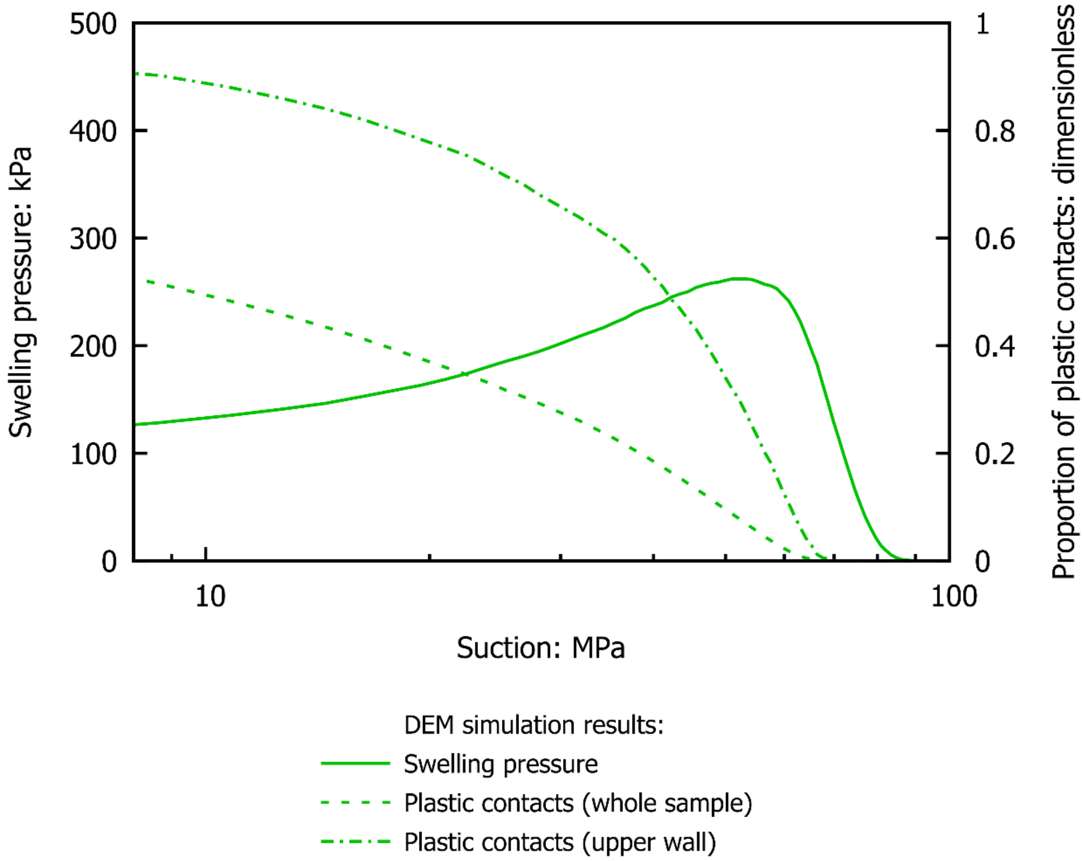

Fig. 12 Coordination number in DEM1, DEM2 and DEM3 simulations (mean values) and evolution of inter-pellet porosity upon suction decrease (identical in all DEM simulations).

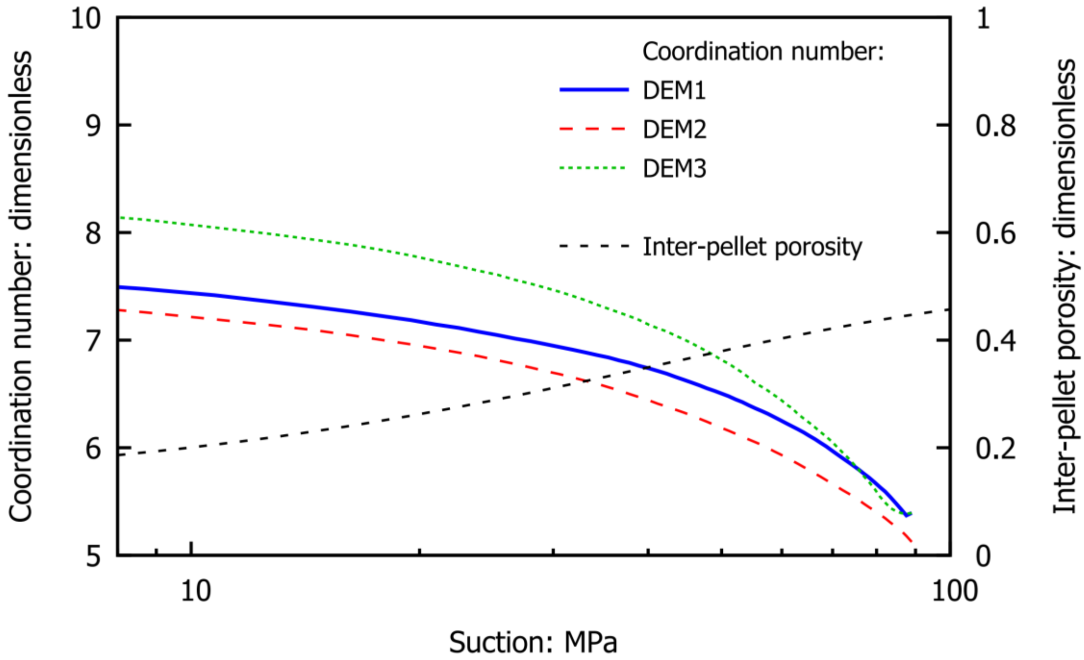

Fig. 13 Coefficient of variation of swelling pressure, proportion of plastic contacts and coordination number in DEM1, DEM2 and DEM3 simulations

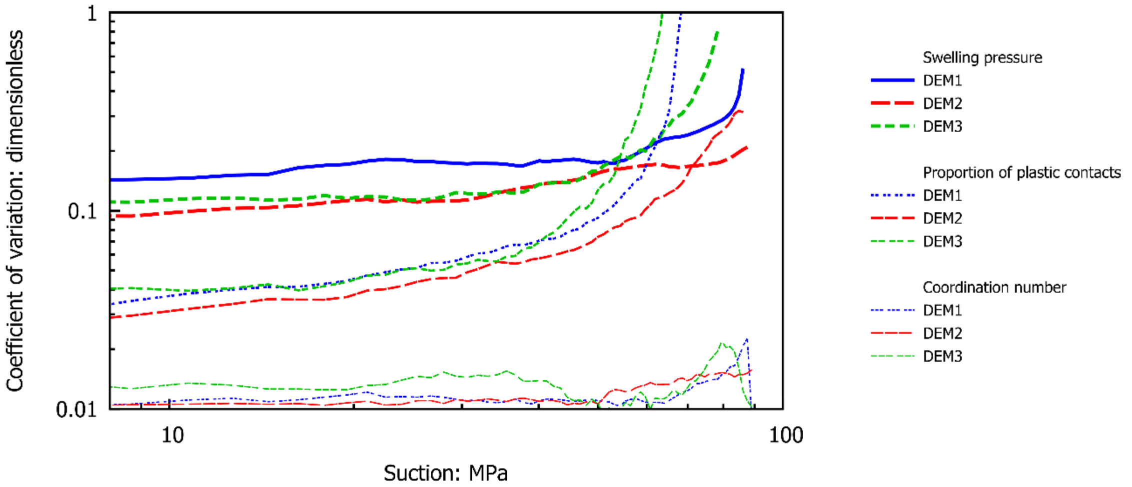

Fig. 14 Variability of the measured swelling pressure in DEM1 simulations for two sensor sizes

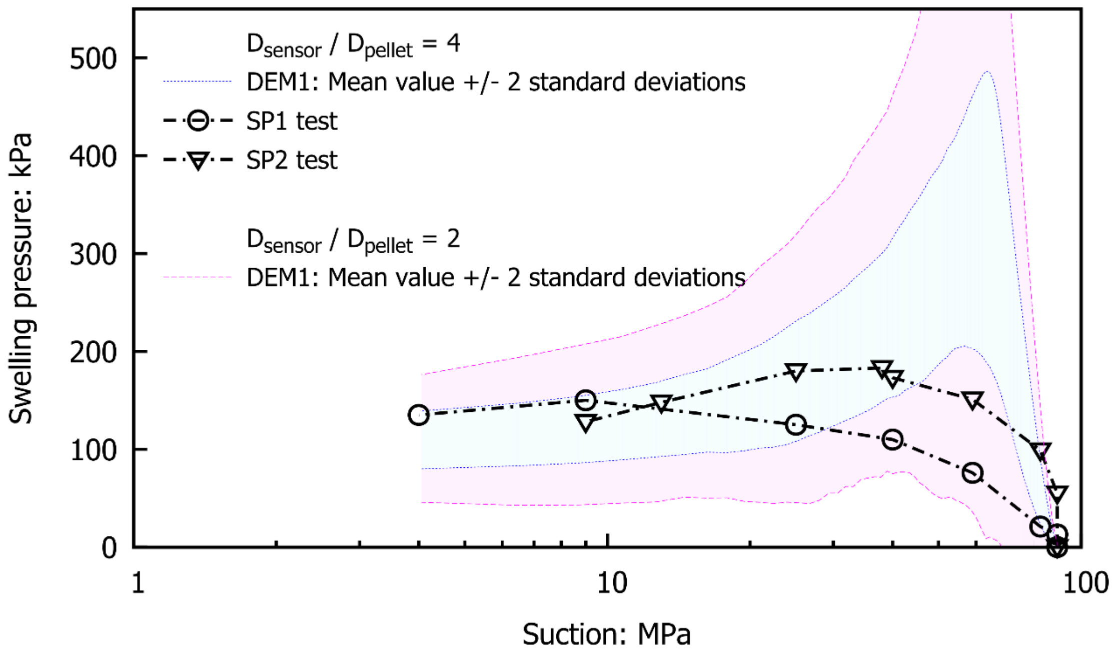

Fig. 15 Coefficient of variation of the measured swelling pressure in DEM1 simulations at peak and at 9 MPa of suction

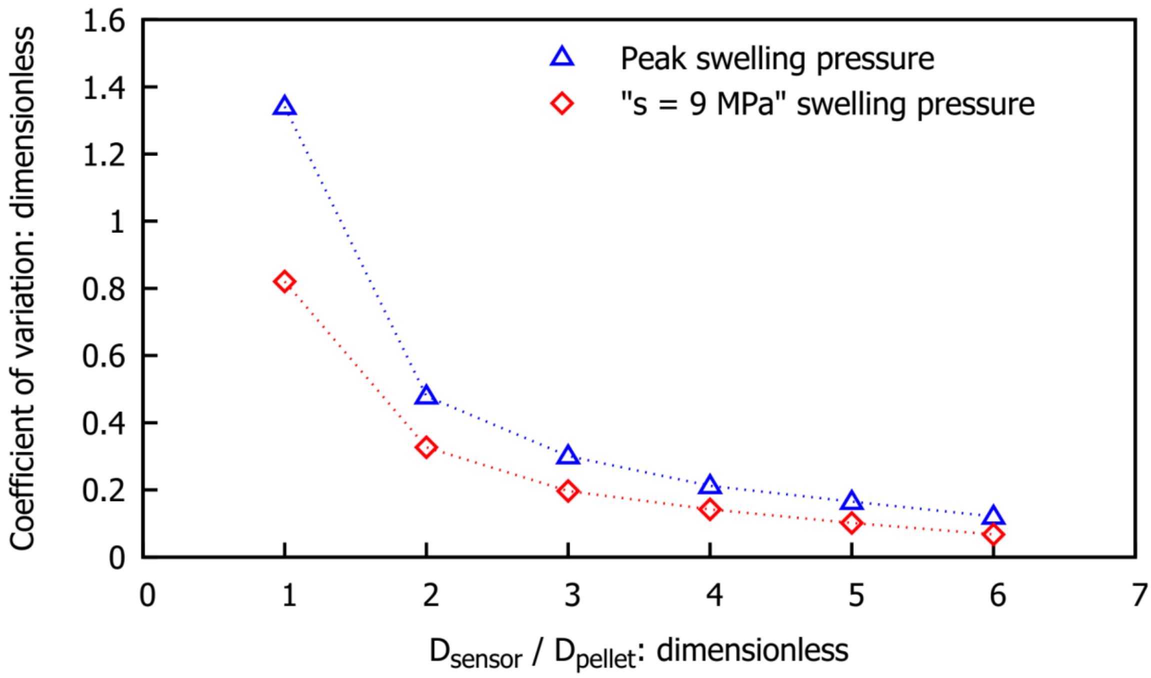

Fig. 16 Evolution of the mean elastic normal deflection in the numerical sample in DEM1, DEM2 and DEM3 simulations. Mean values are plotted

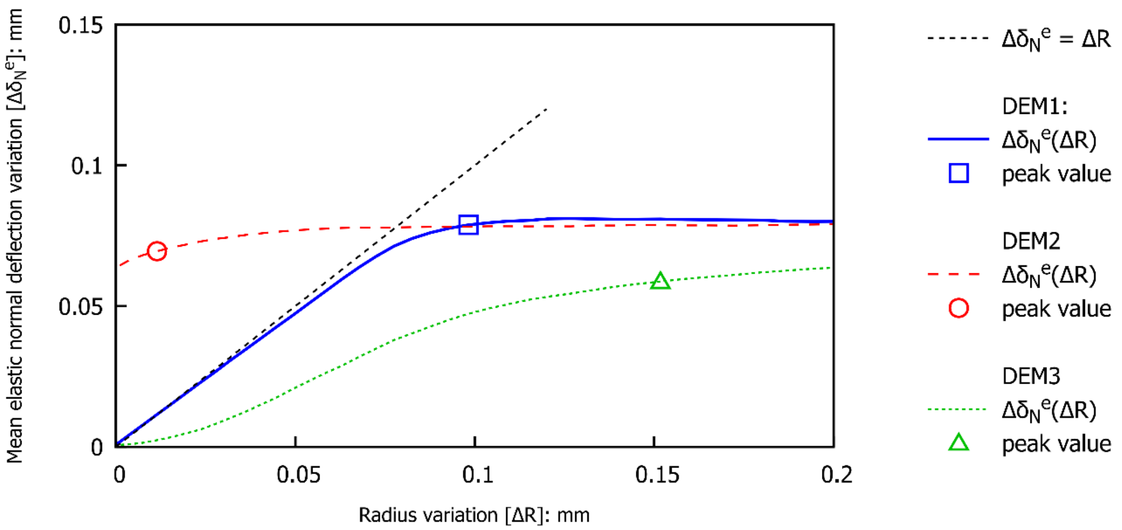

Fig. 17 Comparison of the mean stress calculated in the sample and the swelling pressure measured by the sensor as functions of decreasing suction for DEM1 simulations